Sub- 9 × 29 m, 1.2nW, Fully Digital Potentiostat Design for Dopamine Sensing

Sub-9×29 μm^2, 1.2 nW, Fully Digital Potentiostat Design for Dopamine Sensing

Ali Meimandi, *Student Member, IEEE*, Gian Luca Barbruni, *Member, IEEE*, Paolo Stefano Crovetti, *Senior Member, IEEE,* and Sandro Carrara, *Fellow, IEEE.*

***Abstract*— This paper presents a highly miniaturized and low-power CMOS electrochemical potentiostat based on a fully digital design. The potentiostat functionality has been evaluated through dopamine detection using proper microelectrodes. The system drives an electrochemical cell in a three-electrode configuration and implements the chronoamperometric technique to minimize both power consumption and required area. The circuit has been fabricated using TSMC 180 nm CMOS technology. Supplied at 0.4 V, the potentiostat alone consumes the up-to-date smallest power of 1.2 nW and occupies the up-to-date smallest ever area of 260 μm^2. Together with its voltage reference and oscillator, the entire system consumes 9.2 nW and occupies 370 μm^2. The potentiostatic voltage maintains an accuracy of ±10% (180 mV to 220 mV) for a 200 mV reference and supply voltage ranging from 0.4 V to 0.56 V, at a frequency of 25 kHz, driven by the ring oscillator. In-vitro experiments demonstrate dopamine detection with a sensitivity of 18.74 pulses/μM and a limit of detection of 0.525 μM. Results demonstrate the huge advantage of using the proposed fully-digital design, making this potentiostat well-suited for implantable devices where size and energy efficiency are critical (e.g., Neural Dust).**

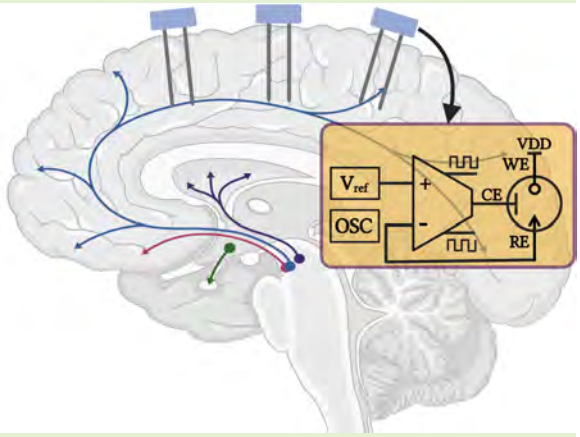

***Index Terms*— CMOS design, Digital Potentiostat, Digital OTA, Electrochemical Sensing, Ultra-Miniaturized and Ultra-Low Power IC, Biomedical Implants, Neural Dust, Body Dust.**

I. Introduction

DOPAMINE (DA) is a neuromodulatory molecule, which plays a critical role in regulating learning, motivation, and movement [1]. Dysregulation or deficiency of DA is correlated to movement and mood disorders, addiction, depression, Parkinson's disease, and schizophrenia [2]. DA concentration can be selectively measured in the striatum, where norepinephrine (electrochemically indistinguishable from DA) concentration is lower [3].

Ultra-miniaturized implants (e.g., Neural Dust [4] and neurograin [5]) are necessary for dopamine sensing due to the need for highly localized and selective measurements in complex brain environments while minimizing tissue damage and immune response. In the case of wirelessly-powered and miniaturized implants with lateral sizes smaller than 100 μm (such as Neural Dust and Body Dust [6]), ultra-low power IC design in the nW range is required.

Conventional analog CMOS potentiostats employ a sensing and a digitalization stage. For the sensing stage, Resistive-feedback Transimpedance Amplifier (R-TIA) [7], [8], [9] and Capacitive-feedback TIA (C-TIA) [10], [11] methods are commonly used. However, the feedback resistor assigns the gain, bandwidth and current noise of the current reader. To detect an nA-pA level current, a linear resistor in the GΩ range is required for a low-power resistive feedback structure. However, the resistor's large size makes full integration on the chip potentiostat challenging and may cause the sensor output to be affected by a significant quantity of thermal noise. On the other hand, the capacitive configuration can diminish the effect of thermal noise and reduce the area with respect to the resistive feedback architecture. Yet, the DC offset from the electrode can saturate the amplifier due to the charge build-up on the capacitor. Alternatively, Current Conveyor (CC) topologies [12]–[14] are used due to their versatility and ability to handle a large input range with high efficiency. The issue with conventional CCs is that they could not achieve simultaneous low quiescent power consumption and large input range since they have a maximum input and output current limited by the dc bias current [15]. Following

Manuscript received Month X, 2024; revised Month X, 2024; accepted Month X, 2024. Date of publication Month X, 2024; date of current version Month X, 2024.

Corresponding author: Gian Luca Barbruni (gian-luca.barbruni@epfl.ch).

A. Meimandi, G.L. Barbruni and S. Carrara are with Bio/CMOS Interfaces Laboratory (BCI), École Polytechnique Fédérale de Lausanne, 2000 Neuchâtel, Switzerland.

Paolo Stefano Crovetti is with the Department of Electronics and Telecommunications (DET), Politecnico di Torino, 10129 Torino, Italy.

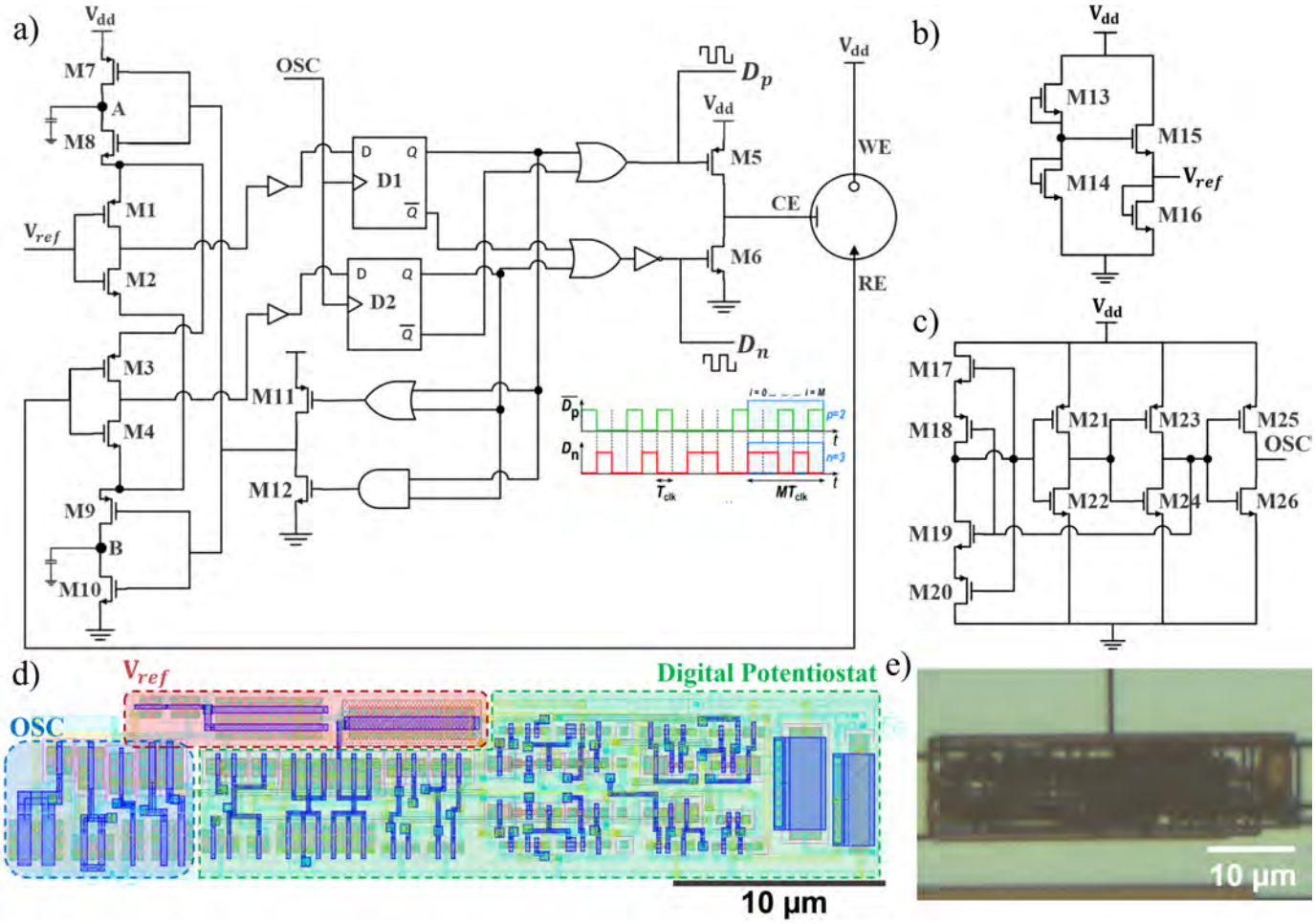

Fig. 1: Schematic of the a) proposed digital potentiostat, consisting of transistors M1–M12, the D Flip-Flops, and associated logic gates. The positive and negative inputs of digital potentiostat are connected to voltage reference and RE respectively. Schematic of the b) 4T voltage reference circuit, and c) ring oscillator. d) System layout, and e) microphotograph of the fabricated circuit.

the sensing stage, a digitalization stage is used thorough Analog-to-Digital Converters (ADCs), such as $\Delta\Sigma$ modulators [16], [17] or Time-to-Digital Converters (TDCs) [18], [19]. While these designs offer straightforward implementations, they come with drawbacks, including high power consumption from the TIA and large area requirements due to the explicit ADC. Alternatively, current-mirror architectures, combined with a current-to-frequency converter (I-F) [18]–[20] have been proposed to eliminate the need for a TIA by directly digitizing the sensor current. However, these approaches suffer from non-linearity, which impact the overall performance. To improve linearity, an additional TDC block is used in the feedback loop. Additionally, all these designs incorporate a control stage to apply the reference voltage, resulting in an increased power and area consumption. Overall, these topologies fail to meet the stringent requirements of ultra-low-power and compact area. Recent sensor-in-the-loop implementations, such as the ultrasensitive amperometric platform by Aymerich et al. [17], integrate sensing and control to achieve self-noise cancellation, offering improved linearity and efficiency. However, these topologies still struggle to meet the ultra-low-power and compact area demands of next-generation implants.

This work addresses these challenges by integrating the sensing, digitization, and control stages into a unified block, employing a digital-based operational transconductance amplifier to effectively reduce both power and area consumption. In our previous work, we presented the potential of the digital potentiostat by showing simulation results for glucose detection, with a circuit consuming 4.7 nW and occupying 460 μm^2 [21]. Building on this preliminary work, this paper demonstrates in-vitro measurements with the fabricated digital CMOS frontend for DA detection, achieving the lowest power consumption, area footprint, and supply voltage ever reported to date in the state-of-the-art.

II. System Design

The CMOS circuit drives an electrochemical cell in a three-electrode configuration for electrochemical detection of the DA. The driving voltage is applied between the Working Electrode (WE) and the Reference Electrode (RE), while the current flows from the WE to the Counter Electrode (CE). Following the conventional approach in amperometric sensing,

the RE is driven by the potentiostat without allowing current flow, ensuring a stable voltage between the WE and the RE. This way, the cell is driven in the right thermodynamic potential to correctly support the redox reaction involving the DA. The driving voltage is kept constant to measure DA concentration in chronoamperometry, with the aim of minimizing both area and power consumption.

The proposed digital potentiostat (Fig.1a) leverages the digital-based amplifier principle [22]. It operates as a digital-based Operational Transconductance Amplifier (OTA) that drives the CE, supplying the necessary current to flow between the CE and WE while maintaining the RE at a constant bias of V_{ref}. If $V_{WE} - V_{RE}$ corresponds to the right Nernst potential (i.e., V_{ref} = 200 mV for DA [23]), the DA concentration is linearly proportional to the faradaic current, and consequently to the number of pulses derived from digital streams of D_p and D_n. For every specific sampling time window (T_{meas}), the average faradaic current I_f is derived by (1):

$$I_f = \frac{nI_n - pI_p}{M} \tag{1}$$

where n and p are the number of pulses respectively generated by D_n and $\overline{D_p}$, and M is the total number of clock cycles driving the logical gates (OSC). I_n and I_p are the currents flowing through M6 and M5 at every clock cycle, respectively. Equation (1) represents the average faradaic current over Tmeas, smoothing out transient fluctuations and quantization noise. When no DA is present ($I_f = 0$), the baseline ratio K_f is derived as the average pulse ratio using (2):

$$0 = \frac{n_0 I_n - p_0 I_p}{M} \Rightarrow K_f = \frac{I_n}{I_p} = \frac{p_0}{n_0} \tag{2}$$

K_f is then used to derive the effective number of pulses N_f proportional to the faradaic current, as an average value using (3):

$$N_f = K_f \times n - p \tag{3}$$

The use of average values in equations (1)–(3) ensures robust DA concentration measurements by mitigating the impact of high-frequency noise and ripple. To establish a 200 mV voltage peak for DA oxidation between the WE and RE, the WE is connected to the system's power supply (V_{dd}) at 400 mV. A V_{ref} = 200 mV voltage is generated by a 4T voltage reference circuit, which is adopted from 2T voltage reference topology [24] (Fig. 1b). V_{ref} is applied to the RE through the negative feedback loop created by the digital potentiostat. The required clock signal for the D Flip-Flops is generated by a three-stage ring oscillator (Fig. 1c), producing a 25 kHz clock at 0.4 V supply voltage via dynamic leakage suppression logic to minimize both area and power consumption [25].

III. Materials and Methods

The CMOS circuit was designed using Cadence Virtuoso 6.1.8.330 and optimized for a supply voltage of 0.4 V to minimize power consumption. Fig. 1d,e respectively show the system layout and its micrograph. Table I reports the transistor sizes for the entire circuit. The latter was fabricated using TSMC 180nm MS/RF/G technology, packaged in a QFN80, and assembled on a testing PCB. For the CMOS

TABLE I: Transistors Sizes (W/L)

Transistor	[$\mu m/\mu m$]	Transistor	[$\mu m/\mu m$]
M1,M2,M3,M4	4.5/0.18	M15[1]	10.4/0.3
M5	1.5/4.4	M16[2]	6/0.6
M6	1/4.4	M17[1]	4/0.6
M7,M8,M9,M10	0.86/0.18	M18[1]	2/0.25
M11	0.8/0.18	M19[1]	2.6/0.3
M12	1.2/0.18	M20[1]	1.32/0.25
M13	1.43/0.18	M21,M22	2/0.18
M14	1.1/0.18	M23[1],M24[1],M25[1],M26[1]	2/0.3

[1]medium threshold voltage transistor [2]3V transistor

measurements, a DC power supply (Keysight E3646A) and an oscilloscope (Keysight MSO-S 804A) were used to evaluate system performance. The digital pulses of D_n and $\overline{D_p}$ were recorded using the oscilloscope and post-processed in MATLAB to derive the effective number of pulses (N_f) using equations 1-3. The power consumption of the system was measured using a source meter (Keysight B2901A). The electrical characterization was performed using a unity-feedback configuration, as illustrated in Fig. 2a, while the experimental setup for electrochemical detection is shown in Fig. 2b.

Platinum/iridium (Pt/Ir) microelectrodes were chosen for their excellent biocompatibility and superior resistance to corrosion and surface degradation, outperforming other metals like tungsten and stainless steel. These properties make Pt/Ir ideal for long-term applications in biological environments [26]. Custom Pt/Ir microelectrodes (Microprobes for Life Science) with exposed tips of 400 μm^2 were used to accommodate the driving current in the current range of the designed digital potentiostat. The microelectrodes were cleaned by sonication in ethanol and deionized water for 5 minutes each. This ensures stable electrochemical performance and limits fouling effects at the start of each measurement session. A standard platinum reference electrode (Metrohm) was used for the electrochemical measurements. Phosphate Buffer Saline (PBS, from Sigma-Aldrich) was prepared with a concentration of 0.01 M phosphate buffer, 0.0027 M potassium chloride, and 0.137 M sodium chloride, pH 7.4, at 25 °C.

Chronoamperometric analysis was conducted using both the fabricated digital potentiostat and the Autolab PGSTAT302N. Dopamine hydrochloride (Sigma-Aldrich) was dissolved in PBS using a magnetic stirrer (Heidolph HeiMix) at 250 rpm to ensure homogeneity. The measurements were conducted by immersing the microelectrodes in the solution while stirring at 250 rpm. Beginning with a PBS-only solution, the DA concentration was increased by 10 μM every 120 seconds. An acquisition time of 120 seconds was initially chosen due to the slow diffusion of species in lab samples. Throughout the measurement period, N_f is calculated continuously. For constructing the calibration curve, N_f is averaged over the

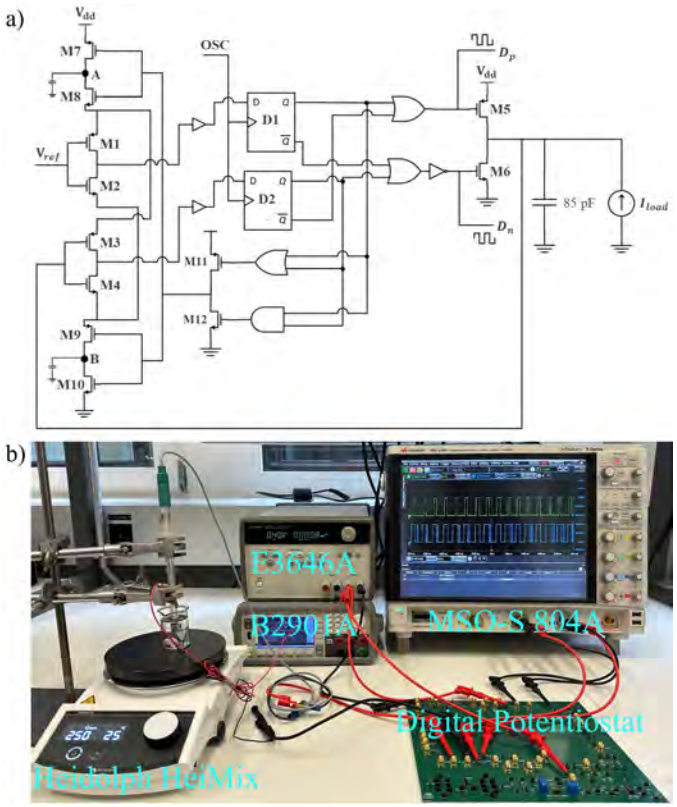

Fig. 2: a) Unity feedback configuration for electrical characterization and b) experimental setup for electrochemical measurement

final 30 seconds of each 120-second interval, once the signal stabilizes, to mitigate transient effects. This approach allowed us to minimize the impact of the slow diffusion of species and capture the steady-state response of the system.

However, brain neurons release and re-absorb DA within a time frame ranging from 10 ms [27] to 5 s [28]. On the other hand, the proposed digital potentiostat offers trade-off between the quantization error and the sensitivity. In other words, the lower T_{meas}, the lower the sensitivity. By considering all these aspects, the sampling time window was set to 100 ms to balance sensitivity and quantization error. This window aligns with sampling rates used in established techniques like Fast-Scan Cyclic Voltammetry (FSCV), which is widely accepted for in vivo DA monitoring [29], [30].

All the above-mentioned experiments were repeated using four different CMOS chips to account for process variations, with standard deviations calculated to assess measurement reliability.

IV. Results and Discussion

A. Electrical Characterization

Fig. 3 presents the transient waveforms of $\overline{Dp}$ (green) and Dn (red) under zero-load current conditions (i.e., $I_f = 0$). By counting the number of pulses p and n during the measurement window and applying Equation (2), the baseline ratio Kf is computed. This, in turn, allows the calculation of the effective number of pulses Nf.

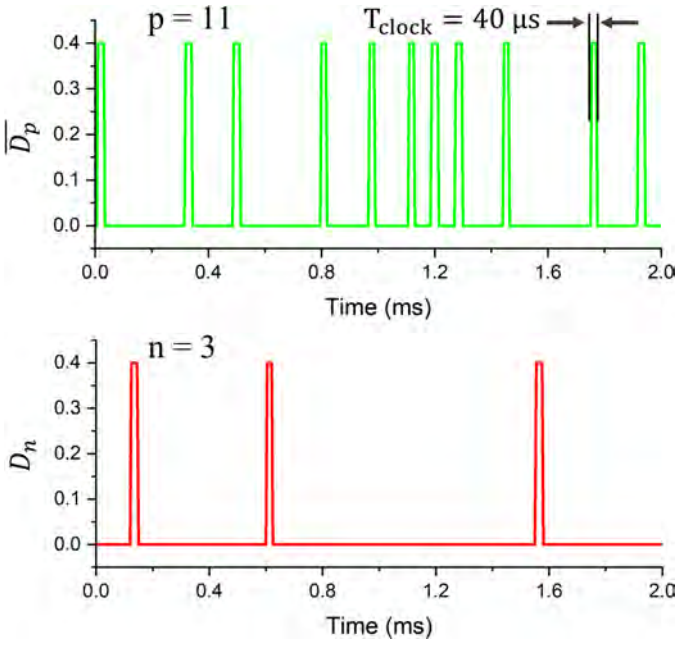

Fig. 3: Transient signal derived from $\overline{D_p}$ and D_n for a zero-load current at a supply voltage of 0.4 V.

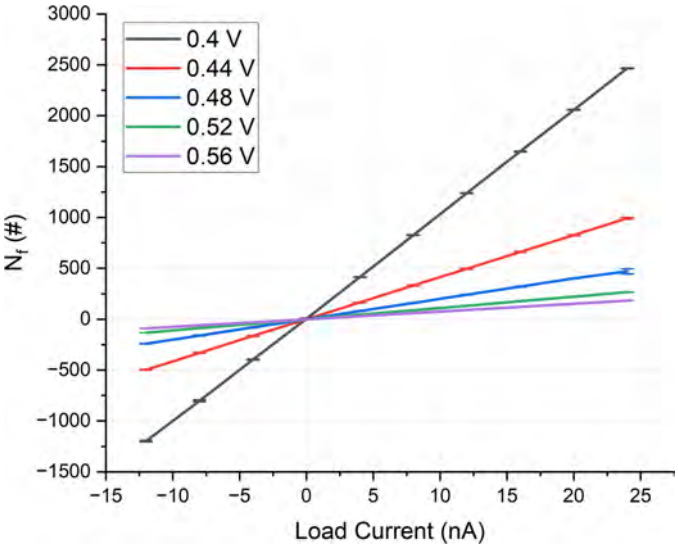

Fig. 4: Effective number of pulses with R^2 = 0.9998 as a function of the load current for supply voltages ranging from 0.4 V to 0.56 V.

Fig. 4 shows N_f as a function of the load current for different supply voltages. N_f remains linear with $R^2 = 0.9998$ for load currents and supply voltages respectively ranging from -12 nA to 24 nA and from 0.4 V to 0.56 V. For every supply voltage, the slope represents the sensitivity of the digital potentiostat. For the nominal and optimized V_{dd} = 0.4 V the sensitivity is 110 pulses/nA, which decreases as V_{dd} increases. Indeed, with a higher V_{dd}, I_n and I_p of (1) increase, resulting in a lower N_f. In addition, the higher the supply voltage, the lower the oscillation frequency of the ring oscillator [25], thus contributing in decreasing the number of pulses in both D_p and D_n. On the other hand, increasing the supply voltage

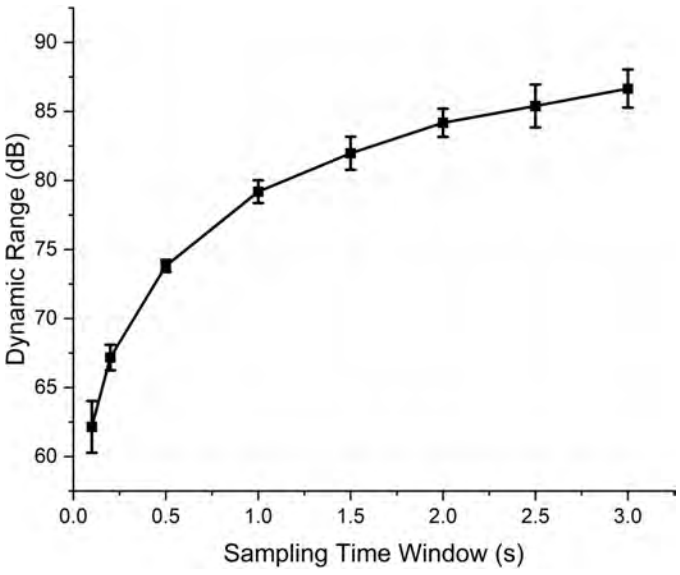

Fig. 5: Dynamic range as a function of the sampling time windows (T_{meas}). The error bars represent the standard deviation of the dynamic range across 300 subsequent measurements.

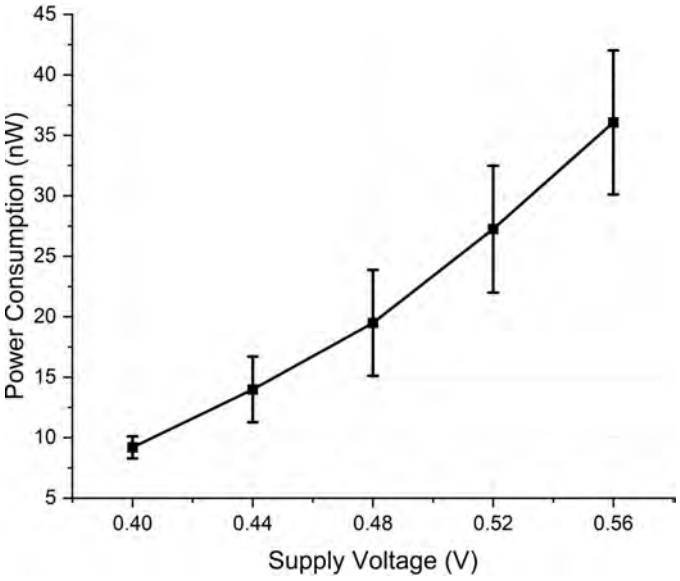

Fig. 6: Power consumption as a function of the supply voltage. The error bars represent the standard deviation across four different chips.

improves the drive strength of the output transistors M5 and M6, resulting in lower variation of the output voltage. Indeed, in unity feedback configuration, the output voltage remains within a range of ±10% of the voltage reference (i.e., from 180 mV to 220 mV) for supply voltages in the range 0.4 V - 0.56 V and load currents in the range from -12 nA to 24 nA.

By considering the nominal sensitivity of the digital potentiostat (Fig. 4, black), the standard deviation of N_f was derived by averaging the measured $\overline{D_p}$ and D_n within T_{meas} for a total of 300 subsequent windows. Therefore, the total input-referred noise (including quantization noise) was derived by dividing the standard deviation of N_f for a zero-load current (i.e., 3.63

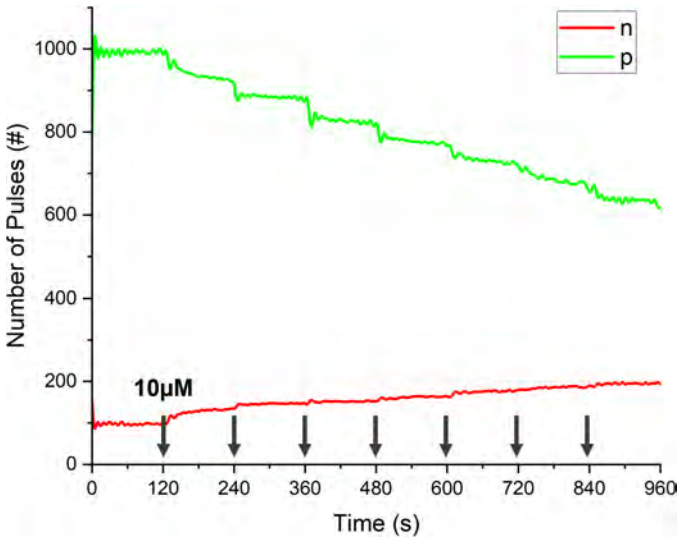

Fig. 7: Number of pulses recorded from gates of transistor M5 (p) and M6 (n) of the digital potentiostat while increasing the DA concentration every 120 seconds.

pulses) over the sensitivity of the digital potentiostat, resulting in 33 pArms. The Dynamic Range (DR) is then derived as in (4):

$$DR = 20 \times \log \frac{Current\ range}{Input\ noise} \tag{4}$$

Fig. 5 shows the potentiostat DR as a function of the time window. The DR is 60 dB for a nominal T_{meas} = 100 ms. By increasing T_{meas}, the quantization noise is reduced, and the sensitivity of the digital potentiostat increases, resulting in a higher DR. In scenarios where T_{meas} can be increased toward 3 seconds, the DR can exceed 85 dB.

Fig. 6 shows the power consumption of the system as a function of the supply voltage. For a nominal V_{dd} = 0.4 V, the entire circuit consumes 9.2 nW, remaining below 45 nW for the maximum V_{dd} = 0.56 V.

B. In-vitro Electrochemical Validation

In DA measurement using the fabricated digital potentiostat, adding DA to the PBS solution increases the faradaic current due to DA's redox reaction at the microelectrodes electrochemical interface. Fig. 7 shows the measured number of pulses at the M5 gate (p, green) and M6 gate (n, red) over a 100 milliseconds window. As expected, the increase in DA concentration results in a higher faradaic current, as in (1), with PMOS sourcing less current and NMOS sinking more current accordingly. Consequently, an increase in pulse count is observed at the NMOS M6 gate, with a corresponding decrease at the PMOS M5 gate to accommodate the increased faradaic current.

Due to the discrete-time nature of the digital feedback loop, the control signals introduce ripple at the reference electrode. However, this ripple is inherently attenuated by the double-layer capacitance (C_{dl}) of the microelectrode–electrolyte interface, which acts as a low-pass filter. The Pt/Ir microelectrodes used in this work exhibit a C_{dl} of approximately 4

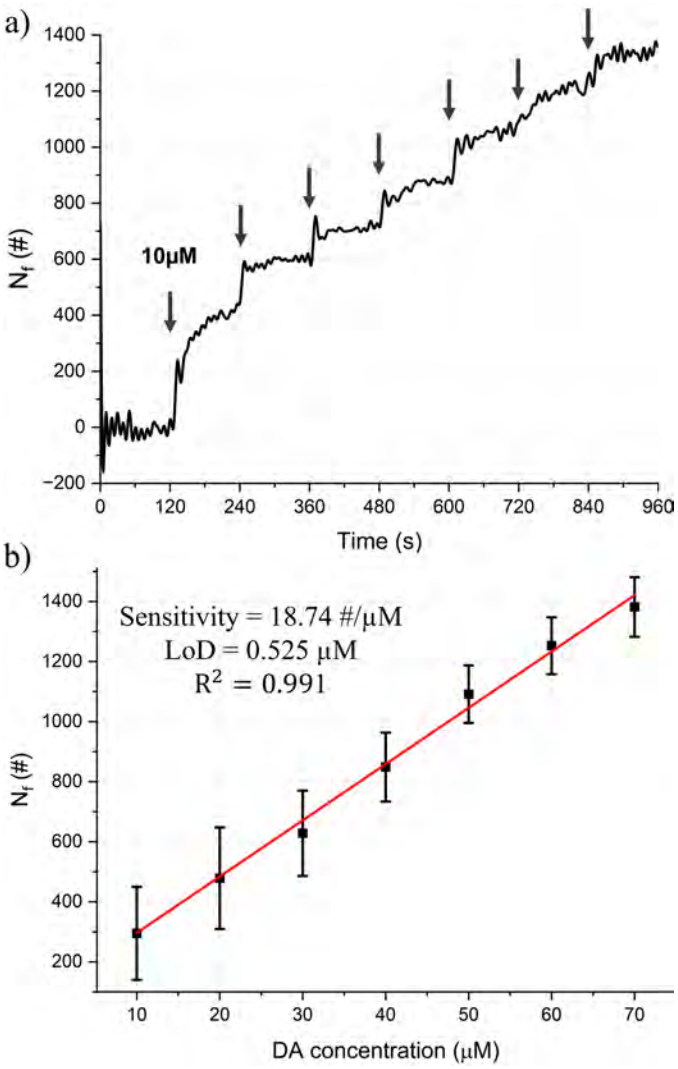

Fig. 8: a) Chronoamperometric measurement of several DA concentrations using microelectrodes and digital potentiostat and b) related calibration curve.

nF, effectively smoothing the high-frequency ripple (25 kHz) introduced by the OTA. As a result, the RE voltage remains stable, ensuring reliable redox operation during the 100 ms chronoamperometric sampling window [31].

Fig. 8a reports N_f as a function of time while increasing the DA concentration. $K_f = 10.09$ was derived by the baseline number of pulses for zero concentration (i.e., If = 0), as in (2).

Fig. 8b shows the derived calibration curve in terms of N_f as a function of the DA concentration. Results highlight a sensitivity of 18.74 pulses/μM and a limit of detection (LoD) of 0.525 μM, with a linearity R^2 of 0.991. The notable drift observed after each dopamine injection in Fig. 8a is primarily attributed to the fouling effect of dopamine [32], which progressively degrades the electrode surface and affects current stability. This phenomenon contributes significantly to the increased standard deviation seen in the calibration curve in Fig. 8b. In addition, various registered noises due to the process variation of the fabricated chip also contribute to the standard deviation of the calibration curve.

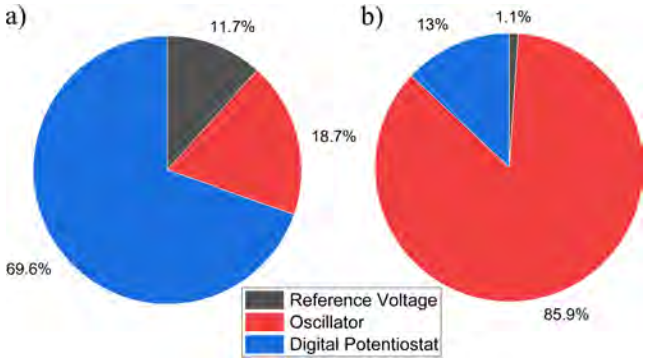

Fig. 9: a) Area and b) power distribution across different blocks of the system.

The same chronoamperometry experiment was performed with the lab instrument, resulting in a maximum measured current of 800 pA, which is in the correct operation range of the digital potentiostat.

Fig. 9a,b respectively show the area and power distribution over the blocks of the system. The latter occupies a total area of 370 μm^2. The digital potentiostat occupies 260 μm^2 only, while the oscillator and the voltage reference circuit occupy 69 μm^2 and 43 μm^2, respectively. The total power consumption of the system is 9.2 nW. The digital potentiostat consumes 1.2 nW only, while the oscillator and voltage reference circuit consume 7.9 nW and 0.1 nW, respectively. It is indeed worth mentioning that 85.9% of the total power consumption is coming from the ring oscillator, due to the used medium threshold voltage transistors for its design. The proposed digital potentiostat architecture allows for future optimization, including lower-power auxiliary blocks and improved scalability in advanced nodes. This work prioritized experimental validation under strict area and power constraints, using a robust ring oscillator at 0.4 V. Future versions could adopt lower-power alternatives such as digital relaxation oscillators [33]. Additionally, the capacitor-less design enables better scaling, as on-chip capacitors do not shrink proportionally with technology nodes and often limit area reduction [34].

Table II compares this work with the state-of-the-art. The measured results are consistent with the simulations previously reported [21], demonstrating that the proposed circuit is three orders of magnitude smaller than the other previously published systems. In addition, the potentiostat alone consumes 1.2 nW, which is the lowest power consumption up-to-date. Akram and collaborators reported a power consumption of 3.72 nW at the cost of a 1000 times larger silicon area [35]. Furthermore, the supply voltage of 0.4 V is significantly smaller than the ones previously reported, making the proposed system optimal for miniaturized and wirelessly-powered implants [36]. This comparison highlights the superiority of this digital design in achieving the lowest power and area consumption, making it highly suitable for Neural Dust [4] and Body Dust [6] applications, where minimizing area and power consumption is key.

TABLE II: State-of-the-art comparison of electronic front-ends for electrochemical sensing

Ref.	Tech. (nm)	Supply (V)	Area (mm^2)	Power (nW)	Current Range (nA)	T_{meas} ms	DR (dB)	Linearity	Topology	Sensing Method	Measured
[18][2]	180	1.2	3.17	19000	-7000 – +10000	0.02	58	0.999	I-F+Count+TDC	CA,CV	Yes
[16][2]	180	1.8	1.6	470000	0 – 105100	10	164.5	-	CT[3]-$\Delta\Sigma$	CA,CV	Yes
[19][2]	180	1.2	0.5	6000	0 – 100000	10	61	0.995	I-F+VCO+TDC	CA	Yes
[35][1]	180	1.2	0.266	3.72	0.08 – 240000	1	129.5	0.998	Comp+Count	CA	Yes
[21][1]	180	0.4	0.00046	4.7	-22 – +33	72	58	0.999	Digital OTA	CA	No
This work[2]	**180**	**0.4**	**0.00037**	**9.2**	**-12 – +24**	**100**	**60**	**0.991**	**Digital OTA**	**CA**	**Yes**
This work[1]			**0.00026**	**1.2**							

[1] Potentiostat only. [2] Total system. [3] Continuous Time.

V. Conclusion

This work presented the smallest ever-fabricated and low-power digital potentiostat, here proposed for dopamine detection. The system has been designed, fabricated, and measured with realistic in-vitro experiments. To evaluate the system's functionality, dopamine sensing was performed using Pt/Ir microelectrodes, demonstrating a sensitivity of 18.74 pulses/μM and a limit of detection of 0.525 μM. The proposed digital approach is the least power-hungry system and the smallest ever potentiostat to date. Occupying just 260 μm^2, and consuming 1.2 nW only at 0.4 V supply voltage, this potentiostat is conceived for implantable biomedical devices targeting neural dust and body dust applications, where power and area consumption are prominent figures of merits. Furthermore, dramatically smaller areas and lower power-hungry circuits can be achieved for sensor front-ends by exploiting this fully digital design approach and utilizing lower CMOS technology nodes.

Acknowledgments

The Authors would like to thank Mrs. Francesca Rodino for her help. This work has received funding from the Swiss State Secretariat for Education, Research, and Innovation (SEFRI) under the contract 22.00025 related to the EU 101046748 CEREBRO project, and under the SwissChips initiative.

References

[1] T. Sippy and N. X. Tritsch, "Unraveling the dynamics of dopamine release and its actions on target cells," *Trends in neurosciences*, vol. 46, no. 3, pp. 228–239, 2023.

[2] S. D. Iversen and L. L. Iversen, "Dopamine: 50 years in perspective," *Trends in neurosciences*, vol. 30, no. 5, pp. 188–193, 2007.

[3] E. W. Schluter, A. R. Mitz, J. F. Cheer, and B. B. Averbeck, "Real-time dopamine measurement in awake monkeys," *PloS one*, vol. 9, no. 6, p. e98692, 2014.

[4] D. Seo, J. M. Carmena, J. M. Rabaey, M. M. Maharbiz, and E. Alon, "Model validation of untethered, ultrasonic neural dust motes for cortical recording," *Journal of neuroscience methods*, vol. 244, pp. 114–122, 2015.

[5] J. Lee, V. Leung, A.-H. Lee, J. Huang, P. Asbeck, P. P. Mercier, S. Shellhammer, L. Larson, F. Laiwalla, and A. Nurmikko, "Neural recording and stimulation using wireless networks of microimplants," *Nature Electronics*, vol. 4, no. 8, pp. 604–614, 2021.

[6] S. Carrara, "Body dust: Well beyond wearable and implantable sensors," *IEEE Sensors Journal*, vol. 21, no. 11, pp. 12 398–12 406, 2020.

[7] L. Wang, C. Zhan, Z. Zhang, and S. Zhao, "A- 40–125° c, 0.8 v, 33 khz relaxation oscillator with integrated voltage and current reference and compensated comparator delay," *Microelectronics Journal*, vol. 117, p. 105285, 2021.

[8] Q. Lin, W. Sijbers, C. Avdikou, D. Gomez, D. Biswas, S. Sneha, A. Malissovas, B. Tacca, and N. Van Helleputte, "21.2 a 22 μw peak power multimodal electrochemical sensor interface ic for bioreactor monitoring," in *2023 IEEE International Solid-State Circuits Conference (ISSCC)*. IEEE, 2023, pp. 314–316.

[9] K.-D. You, E. Cuniberto, S.-C. Hsu, B. Wu, Z. Huang, X. Pei, and D. Shahrjerdi, "An electrochemical biochip for measuring low concentrations of analytes with adjustable temporal resolutions," *IEEE Transactions on Biomedical Circuits and Systems*, vol. 14, no. 4, pp. 903–917, 2020.

[10] S. R. Kumashi, D. Jung, J. Park, S. T. Sanz, S. Grijalva, A. Wang, S. Li, H. C. Cho, C. M. Ajo-Franklin, and H. Wang, "A CMOS multi-modal electrochemical and impedance cellular sensing array for massively paralleled exoelectrogen screening," *IEEE Transactions on Biomedical Circuits and Systems*, vol. 15, no. 2, pp. 221–234, 2021.

[11] A. Meimandi, P. Feng, M. Carminati, T. G. Constandinou, and S. Carrara, "Implantable biosensor for brain dopamine using microwire-based electrodes," in *2023 IEEE BioSensors Conference (BioSensors)*. IEEE, 2023, pp. 1–4.

[12] S. Sarkar and A. Anand, "An integrated multipurpose low-power electrochemical readout interface with on-chip input waveform generator," in *2024 37th International Conference on VLSI Design and 2024 23rd International Conference on Embedded Systems (VLSID)*. IEEE, 2024, pp. 174–179.

[13] D. Ying, J. Rosenberg, N. K. Singh, and D. A. Hall, "A 26.5 pa rms neurotransmitter front-end with class-ab background subtraction," *IEEE Transactions on Biomedical Circuits and Systems*, vol. 16, no. 4, pp. 692–702, 2022.

[14] S. Kang, B. Jin, M. Yoo, H. Son, K. Kim, J. Wi, G. Nam, N. H. Bae, Y. M. Park, J. H. Jang *et al.*, "Low-noise and process variation-tolerant readout circuit for electrochemical sensors," *IEEE Sensors Journal*, 2024.

[15] D. Ying and D. A. Hall, "Current sensing front-ends: A review and design guidance," *IEEE Sensors Journal*, vol. 21, no. 20, pp. 22 329–22 346, 2021.

[16] J. Yeom, H. Kim, W. Jeong, W. Cho, T. Kim, S. Bag, Y. Kim, Y. Lee, H. Shin, and J. J. Kim, "A potentiostat-based wide-DR multi-sensor integrated interface for heterogeneous chemical sensor applications," *IEEE Transactions on Circuits and Systems II: Express Briefs*, 2024.

[17] J. Aymerich, A. Ferrer-Vilanova, J. Cisneros-Fernández, R. Escudé-Pujol, G. Guirado, L. Terés, M. Dei, X. Muñoz-Berbel, and F. Serra-Graells, "Ultrasensitive bacterial sensing using a disposable all-in-one amperometric platform with self-noise cancellation," *Biosensors and Bioelectronics*, vol. 234, p. 115342, 2023.
[18] S.-Y. Lu and Y.-T. Liao, "A 19 μw, 50 ks/s, 0.008-400 v/s cyclic voltammetry readout interface with a current feedback loop and on-chip pattern generation," *IEEE Transactions on Biomedical Circuits and Systems*, vol. 15, no. 2, pp. 190–198, 2021.
[19] S. Yu, T.-H. Chou, S. Bose, J. Cook, J. Park, and M. L. Johnston, "A reconfigurable tri-mode frequency-locked loop readout circuit for biosensor interfaces," *IEEE Transactions on Biomedical Circuits and Systems*, vol. 17, no. 4, pp. 768–781, 2023.
[20] S.-Y. Lu, S.-S. Shan, C.-Z. Shao, T.-H. Lu, Y.-H. Yeh, I.-T. Lin, S.-P. Lin, and Y.-T. Liao, "Wireless multimodality sensing system-on-a-chip with time-based resolution scaling technique and analog waveform generator in 0.18 μm CMOS for chronic wound care," *IEEE Transactions on Biomedical Circuits and Systems*, vol. 15, no. 6, pp. 1268–1282, 2021.
[21] R. Rubino, S. Carrara, and P. Crovetti, "Direct digital sensing potentiostat targeting body-dust," in *2022 IEEE Biomedical Circuits and Systems Conference (BioCAS)*. IEEE, 2022, pp. 280–283.
[22] P. Toledo, R. Rubino, F. Musolino, and P. Crovetti, "Re-thinking analog integrated circuits in digital terms: A new design concept for the iot era," *IEEE Transactions on Circuits and Systems II: Express Briefs*, vol. 68, no. 3, pp. 816–822, 2021.
[23] D. N. Oko, S. Garbarino, J. Zhang, Z. Xu, M. Chaker, D. Ma, D. Guay, and A. C. Tavares, "Dopamine and ascorbic acid electro-oxidation on au, aupt and pt nanoparticles prepared by pulse laser ablation in water," *Electrochimica Acta*, vol. 159, pp. 174–183, 2015.
[24] M. Seok, G. Kim, D. Blaauw, and D. Sylvester, "A portable 2-transistor picowatt temperature-compensated voltage reference operating at 0.5 v," *IEEE Journal of Solid-State Circuits*, vol. 47, no. 10, pp. 2534–2545, 2012.
[25] A. Meimandi, G. L. Barbruni, and S. Carrara, "A 69 μm 2 sub-nw/khz capacitor-less ring oscillator for ultra-miniaturized implants," in *2024 13th International Conference on Modern Circuits and Systems Technologies (MOCAST)*. IEEE, 2024, pp. 01–04.
[26] A. Prasad, Q.-S. Xue, R. Dieme, V. Sankar, R. C. Mayrand, T. Nishida, W. J. Streit, and J. C. Sanchez, "Abiotic-biotic characterization of pt/ir microelectrode arrays in chronic implants," *Frontiers in neuroengineering*, vol. 7, p. 2, 2014.
[27] S. E. Hochstetler, M. Puopolo, S. Gustincich, E. Raviola, and R. M. Wightman, "Real-time amperometric measurements of zeptomole quantities of dopamine released from neurons," *Analytical chemistry*, vol. 72, no. 3, pp. 489–496, 2000.
[28] W. G. Kuhr and R. M. Wightman, "Real-time measurement of dopamine release in rat brain," *Brain research*, vol. 381, no. 1, pp. 168–171, 1986.
[29] B. J. Venton and Q. Cao, "Fundamentals of fast-scan cyclic voltammetry for dopamine detection," *Analyst*, vol. 145, no. 4, pp. 1158–1168, 2020.
[30] L. C. Kimble, J. S. Twiddy, J. M. Berger, A. G. Forderhase, G. S. McCarty, J. Meitzen, and L. A. Sombers, "Simultaneous, real-time detection of glutamate and dopamine in rat striatum using fast-scan cyclic voltammetry," *ACS sensors*, vol. 8, no. 11, pp. 4091–4100, 2023.
[31] A. Meimandi, G. L. Barbruni, and S. Carrara, "A more reliable equivalent circuit of electrochemical sensors for robust design of cmos front-ends," *IEEE Sensors Journal*, 2025.
[32] E. Peltola, S. Sainio, K. B. Holt, T. Palomaki, J. Koskinen, and T. Laurila, "Electrochemical fouling of dopamine and recovery of carbon electrodes," *Analytical chemistry*, vol. 90, no. 2, pp. 1408–1416, 2018.
[33] O. Aiello, P. Crovetti, L. Lin, and M. Alioto, "A pw-power hz-range oscillator operating with a 0.3–1.8-v unregulated supply," *IEEE Journal of Solid-State Circuits*, vol. 54, no. 5, pp. 1487–1496, 2019.
[34] H. Yin, E. Ashoori, X. Mu, and A. J. Mason, "A compact low-power current-to-digital readout circuit for amperometric electrochemical sensors," *IEEE transactions on instrumentation and measurement*, vol. 69, no. 5, pp. 1972–1980, 2019.
[35] M. A. Akram, A. Aberra, S.-J. Kweon, and S. Ha, "3.6 an amplifier-less CMOS potentiostat ic consuming 3.7 nw power all over 129.5 db dynamic range for electrochemical biosensing," in *2024 IEEE International Solid-State Circuits Conference (ISSCC)*, vol. 67. IEEE, 2024, pp. 64–66.
[36] G. L. Barbruni, P. M. Ros, D. Demarchi, S. Carrara, and D. Ghezzi, "Miniaturised wireless power transfer systems for neurostimulation: A review," *IEEE Transactions on Biomedical Circuits and Systems*, vol. 14, no. 6, pp. 1160–1178, 2020.

Ali Meimandi (Graduate Student Member, IEEE) received B.Sc degree in electrical engineering from Amirkabir University of Technology(Tehran Polytechnic), Tehran, Iran, and M.Sc. degree in electronic engineering from Politecnico di Milano, Milan, Italy, in 2018 and 2022, respectively. He is currently pursuing the Ph.D. degree at the Bio/CMOS Interfaces Laboratory (BCI) from École Polytechnique Fédérale de Lausanne (EPFL), Neuchâtel, Switzerland. His research is focused on designing and implementing ultralow power and Ultralow area analog/mixed-signal IC for brain monitoring. His current research interests include electronic systems for sensor front-ends, neural prostheses, analog and digital CMOS design, ultra-low-power, and miniaturized CMOS integrated circuits.

Gian Luca Barbruni (S'20-M'24) was born in Sanremo (IM), Italy, in 1995. He received his B.Sc. and M.Sc. degrees in Biomedical Engineering from Politecnico di Torino, Turin, Italy, in 2017 and 2019, respectively. He worked as a Research Associate with the Department of Electronics and Telecommunications (DET) and the MiNES (Micro & Nano Electronic Systems) Laboratory at Politecnico di Torino. In 2023, he obtained his Ph.D. in Microelectronics and Microsystems from École Polytechnique Fédérale de Lausanne (EPFL), Switzerland, with a focus on the design and development of innovative cortical visual prostheses for vision restoration in the blind. Currently, he is a Principal Investigator and postdoctoral researcher at the Bio/CMOS Interfaces Laboratory in Neuchâtel, EPFL. Dr. Barbruni's research focuses broadly on designing novel wearable and implantable devices that combine low-power mixed-signal IC design, wireless power transfer and energy harvesting, as well as post-CMOS processing and microfabrication techniques, all aimed at advancing continuous monitoring systems and brain-computer interfaces.

Paolo S. Crovetti (S'00-M'04-SM'20) was born in Turin, Italy, in 1976. He received the Laurea (summa cum laude) and Ph.D. degrees in electronic engineering from the Politecnico di Torino, Turin, Italy, in 2000 and 2003, respectively. He is currently an Associate Professor with the Department of Electronics and Telecommunications (DET), Politecnico di Torino, Turin where he leads a research group in Analog, Mixed-Signal and Power microelectronics with several international collaborations and teaches courses on basic and automotive electronics. He has co-authored more than 110 papers appearing in journals and international conference proceedings. His main research interests are in the fields integrated circuit design and electromagnetic compatibility (EMC). His recent research activities are focused on non-conventional, digital-based information processing techniques and ultra-low-voltage, ultra-low-power IC design for the Internet of Things and next-generation biosensors. Prof. Crovetti is a co-recipient of the PRIME23 Gold Leaf Prize, of the Best Student Paper Award at the 26th IEEE International Conference on Electronics Circuits and Systems (ICECS) in 2018 and of the Excellent Paper Award at the 2009 International Symposium on EMC, Kyoto. Prof. Crovetti serves as the Editor-in-Chief of IET Electronics Letters and as an Associate Editor of the IEEE TRANSACTIONS ON CIRCUITS AND SYSTEMS - Part I Regular Papers and of the IEEE TRANSACTIONS ON VERY LARGE SCALE OF INTEGRATION, and is the co-Chair of the EMC Society Italy Chapter.

Sandro Carrara (F'15) is an IEEE Fellow and also the recipient of the IEEE Sensors Council Technical Achievement Award in 2016, and the Scientist Medal by the International Association of Advanced Materials in 2024. He is Professor at the EPFL in Lausanne (CH), and former professor at the Universities of Genoa and Bologna (IT). He holds a PhD in Biochemistry and Biophysics from University of Padua (IT), a master degree in physics from University of Genoa (IT), and a diploma in Electronics from National Institute of Technology in Albenga (IT). Along his career, he published 7 books with prestigious publishers such as Springer/NATURE and Cambridge University Press. He has more than 400 scientific publications and is author of 19 patents/patent-requests. He is former Editor-in-Chief of the IEEE Sensors Journal, one of the largest journals among 220 IEEE publications, and Associate Editor of IEEE Transactions on Biomedical Circuits and Systems. He is also former Founding Editor-in-Chief of the Springer/NATURE journal titled NanoBioScience. He is a member of the IEEE Sensors Council and his Executive Committee. He was a member of the Board of Governors (BoG) of the IEEE Circuits And Systems Society (CASS). He has been appointed as CASS Distinguished Lecturer for the years 2013-2014, and IEEE Sensors Council Distinguished Lecturer for the years 2017-2019. His work has constantly received international recognition with several best-cited papers and best conference papers. He has been the General Chairman of the premier worldwide international conference in the area of circuits and systems for biomedical applications, IEEE BioCAS, in 2014. He also has been the General Chairman of the 16th Edition of IEEE International Symposium on Medical Measurements and Applications, IEEE MeMeA, in 2021.